ISSN 1674-1056
http://cpb.iphy.ac.cn
http://iopscience.iop.org/cpb
中国物理 B
Chinese Physics
中国物理 Chinese Physics B

Characteristic plume morphologies of atmospheric Ar and He plasma jets excited by a pulsed microwave hairpin resonator

Zhao-Quan Chen(陈兆权), Ben-Kuan Zhou(周本宽), Huang Zhang(张煌), Ling-Li Hong(洪伶俐), Chang-Lin Zou(邹长林), Ping Li(李平), Wei-Dong Zhao(赵卫东), Xiao-Dong Liu(刘晓东), Olga Stepanova, A A Kudryavtsev

Citation: Chin. Phys. B . 2018, 27(5): 055202. **doi:** 10.1088/1674-1056/27/5/055202

Journal homepage: http://cpb.iphy.ac.cn; http://iopscience.iop.org/cpb

What follows is a list of articles you may be interested in

Sterilization of mycete attached on the unearthed silk fabrics by an atmospheric pressure plasma jet

Rui Zhang(张锐), Jin-song Yu(於劲松), Jun Huang(黄骏), Guang-liang Chen(陈光良), Xin Liu(刘欣), Wei Chen(陈维), Xing-quan Wang(王兴权), Chao-rong Li(李超荣)

Chin. Phys. B . 2018, 27(5): 055207. **doi:** 10.1088/1674-1056/27/5/055207

Numerical study of the effect of water content on OH production in a pulsed-dc atmospheric pressure helium-air plasma jet

Mu-Yang Qian(钱沐杨), Cong-Ying Yang(杨从影), Zhen-dong Wang(王震东), Xiao-Chang Chen(陈小昌), San-Qiu Liu(刘三秋), De-Zhen Wang(王德真)

Chin. Phys. B . 2016, 25(1): 015202. **doi:** 10.1088/1674-1056/25/1/015202

A two-dimensional model of He/O_2 atmospheric pressure plasma needle discharge

Qian Mu-Yang, Yang Cong-Ying, Chen Xiao-Chang, Liu San-Qiu, Yan Wen, Liu Fu-Cheng, Wang De-Zhen

Chin. Phys. B . 2015, 24(12): 125203. **doi:** 10.1088/1674-1056/24/12/125203

Pulsed microwave-driven argon plasma jet with distinctive plume patterns resonantly excited by surface plasmon polaritons

Chen Zhao-Quan, Yin Zhi-Xiang, Xia Guang-Qing, Hong Ling-Li, Hu Ye-Lin, Liu Ming-Hai, Hu Xi-Wei, A. A. Kudryavtsev

Chin. Phys. B . 2015, 24(2): 025203. **doi:** 10.1088/1674-1056/24/2/025203

Three different low-temperature plasma-based methods for hydrophilicity improvement of polyethylene films at atmospheric pressure

Chen Guang-Liang, Zheng Xu, Huang Jun, Si Xiao-Lei, Chen Zhi-Li, Xue Fei, Sylvain Massey

Chin. Phys. B . 2013, 22(11): 115206. **doi:** 10.1088/1674-1056/22/11/115206

Characteristic plume morphologies of atmospheric Ar and He plasma jets excited by a pulsed microwave hairpin resonator*

Zhao-Quan Chen(陈兆权)[1,†], Ben-Kuan Zhou(周本宽)[1], Huang Zhang(张煌)[1], Ling-Li Hong(洪伶俐)[1], Chang-Lin Zou(邹长林)[1], Ping Li(李平)[1], Wei-Dong Zhao(赵卫东)[1], Xiao-Dong Liu(刘晓东)[1], Olga Stepanova[2], and A A Kudryavtsev[2]

[1] *School of Electrical & Information Engineering, Anhui University of Technology, Maanshan* 243032, *China*
[2] *Faculty of Physics, St. Petersburg State University, St. Petersburg* 198504, *Russia*

(Received 17 January 2018; revised manuscript received 12 February 2018; published online 26 April 2018)

Different discharge morphologies in atmospheric Ar and He plasmas are excited by using a pulsed microwave hairpin resonator. Ar plasmas form an arched plasma plume at the opened end of the hairpin, whereas He plumes generate only a contracted plasmas in between both tips of metal electrodes. Despite this different point, their discharge processes have three similar characteristics: (i) the ionization occurs at the main electrode firstly and then develops to the slave electrode, (ii) during the shrinking stage the middle domain of the discharge channels disappears at last, and (iii) even at zero power input (in between pulses) a weak light region always exists in the discharge channels. Both experimental results and electromagnetic simulations suggest that the discharge is resonantly excited by the local enhanced electric fields. In addition, Ar ionization and excitation energies are lower than those of He, the effect of Ar gas flow is far greater than that of He gas, and the contribution of accelerated electrons only locates at the domain with the strongest electric fields. These reasons could be used to interpret the different characteristic plume morphologies of the proposed atmospheric Ar and He plasmas.

Keywords: atmospheric pressure plasma jet, pulsed microwave discharge, surface plasmon polaritons, hairpin resonant discharge

PACS: 52.35.Mw, 52.50.Sw, 52.40.Fd **DOI:** 10.1088/1674-1056/27/5/055202

1. Introduction

Characteristic discharge morphologies richly exist in atmospheric pressure plasma jet (APPJ) plumes, whose formation mechanism has been focused on because of its attractive prospective in theoretical research and industrial applications.[1,2] In the past decade, APPJ plumes generated by a pulsed DC power supply or low-frequency voltages were often observed as discrete bullet-shaped fronts moving along with the jet axis, instead of luminous plasma jet plumes watched by the naked eye.[3] Most of them were applied with noble gases like Ar or He as working gas. For kHz Ar and He APPJ plumes, the similar plume formations were often exhibited besides that He plasma formed a longer and more stable plasma jet plume in comparison with Ar plasma. When the frequency of the applied voltages increases to radio frequency, the Ar APPJ plume will become a radial contraction and filamentary, while He plasma jet will be constricted to the electrodes.[4] The reasons for the changeable formation have been extensively researched. The main influence factors are attributed to the dominant ionization processes. Ar plasmas are included in stepwise ionization and He plasmas are known to be direct ionization. Sometimes Penning ionization might play an important role in the formation of distinctive morphologies.[5–11] Generally speaking, He plasmas are always with good performances, like lower breakdown voltage, higher portion of reactive species, more safety in electrical shock and room gas temperature, in comparison to Ar plasmas. In view of engineering applications, He plasmas are more favorable than Ar plasmas at the applied frequency lower than radio frequency.

To focus more attention on APPJ's morphologies varying with the applied frequency, formations of microwave (2.45 GHz) APPJ plumes have been adequately studied. Munoz and Calzada[12] have studied the influence of the He proportion on the radial contraction of the Ar plasma in a surface-wave plasma setup. Takamura *et al.*[13] have investigated the formation and decay processes of Ar/He microwave plasma jet. It was found that the gas flow turbulence and the recombination rate influenced the decay speed of plasma column at a power shut-off stage. Chen *et al.*[14,15] have shown the filamentary streamer discharges excited by the enhanced microwave resonator of surface plasmon polaritons (SPPs). Hnilica *et al.*[16] have experimented on the characterization of a periodic instability in filamentary surface wave discharge at atmospheric pressure in Ar gas. Chen *et al.*[17] have researched the propagation characteristics of a pulse-modulated

*Project supported by the National Natural Science Foundation of China (Grant Nos. 11575003 and 51607003).
†Corresponding author. E-mail: qq66168@163.com
© 2018 Chinese Physical Society and IOP Publishing Ltd

surface-wave APPJ Ar plume. Lee *et al.*[4,18,19] have reported a type of discharge formation in Ar and He plasmas by using coaxial transmission line resonators (CTLR). Ar plasmas exhibited plasma jet plumes with contracted and filamentary formation, whereas He plasmas formed only constricted plasmas, as the frequency varied from 0.9 GHz to 2.45 GHz. Recently, Chen *et al.*[20,21] have obtained the bullet-shaped ionization front and the donut shape cross section of Ar APPJ plumes but only a confined He plasma by adopting a CTLR driven by microwave pulses.

However, these previous works mainly focused on the distinctive discharge morphologies and its formation processes with no electrodes (surface-wave discharges[12–17]) or a signal powered electrode (CTLR discharges[18–21]). As for the resonated discharges between two electrodes, Hopwood *et al.*[22–29] have investigated the microplasma structure and lifetime of the electrodes to microstrip line resonators with a discharge gap of about 100 μm. Although the frequency-scale rule can regulate the characteristic of microwave discharges between both electrodes, a dielectric surface might influence the formation structure of the discharge because both electrodes of microstrip line resonators are posted on a printed circuit board. Moreover, Kang *et al.*[30] have reported a slit shaped microwave atmospheric pressure plasma based on a parallel plate transmission line resonator with a gap of 0.2 mm. For overcoming the shortcut of a small gap, Chen *et al.*[31] have proposed a microwave discharge in a free-space gap of 2 mm between both electrodes generated by a hairpin resonator. The plasma jet plume of the hairpin resonator performs distinctive formations, like an arched plasma pattern and local plasma bullets, and the radian of the arched plasma plume is mainly influenced by the input power and Ar gas flow rate. Therefore, in order to further investigate the formation mechanism of microwave discharge at a larger free-space gap between two powered electrodes, the present study is mainly focused on the ionization process and the characteristic morphologies of atmospheric Ar and He plasmas excited by a pulsed microwave hairpin resonator.

2. Experimental setup and operations

Figure 1 shows the schematic of the hairpin resonator and its discharge images. The proposed hairpin resonator is with a U-shaped powered electrode as shown in Fig. 1(a). Due to the applied microwave frequency of 2.45 GHz, the wavelength in free space equals to 122.4 mm and three quarters of the wavelength approximates to 92 mm. Thence the total length of the U-shaped powered electrode is 45 mm and the whole length of powered metal wire is 92 mm (45 mm$\times$2 + 2 mm= 92 mm). The U-shaped powered electrode is located at the center of a quartz tube. The length of the quartz tube is 55 mm. The inner and outer diameters of the quartz tube are 4 mm and 6 mm, respectively. The hairpin resonator is powered through a Sub-Miniature-A connector, while the distance between the power excitation point and the opened end of U-shape powered electrode is about 31 mm (a quarter of the wavelength). This structure can make sure that the maximum voltage locates at the opened side.[32,33] The tip of one powered metal wire is with positive maximum voltage, and meanwhile the tip of the opposite powered metal wire has negative maximum voltage. Adding the tips of the metal wire being sharpened to about 0.05 mm, the strongest electric field is placed at the opened side of the U-shaped powered electrode. A piece of copper glue film is pasted around the outer surface of the quartz tube (acted as grounded electrode). A pulse microwave power supply drives the hairpin resonator, which is composed of a pulsed signal modulator (5 V pulse square wave with frequency of 10 Hz–200 kHz and duty ratio of 0.01–0.99), a microwave signal generator (frequency of 2.4–2.5 GHz, output power of 100 mW, 2.45 GHz used in the present study), and a 48 dB power amplifier (continued power output adjusted from 0 to 60 W, each pulse with a rise time velocity about 1 W/μs, and a linear fall-time velocity of 25 W/μs).

Ar gas (or He gas) with 99.999% purity is used as working gas. The gas flow is controlled by a valve controller which can change from 0 to 10 slm and monitored by a gas flow meter (MF5700R). As shown in Fig. 1(a), the working gas is input to the hairpin resonator and ejects from the opened nozzle of the quartz tube into ambient air finally. When the pulsed microwave power higher than 2 W and the working gas flow of 1 slm are applied on the hairpin resonator, the discharge will take place at the opened end of the U-shaped powered electrode. Different working gases will induce different discharge image patterns. Ar plasmas form an arched plasma plume at the opened end of the hairpin resonator, whereas He plumes generate only contracted plasmas in between both tips of the U-shaped powered electrode, as shown in Fig. 1(b). In the experiment, the time with pulsed microwave power is normally about several tens of microseconds; however, the shortest exposure time of a digital camera (Canon EOS 60D) is merely 0.125 ms. Thence the photo images taken by the Canon EOS 60D camera cannot apply to distinguish the ionization process. In the present experiment, a fast-gated Andor ICCD camera (iStar performance sheet DH340T, pixels: 2048$\times$512, minimum optical gate: 1.9 ns, exposure time in the span of 1.9 ns–10 s) is used to capture the discharge images, which is triggered externally by the same signal channel of the pulsed modulator in order to synchronize with the discharge generation.

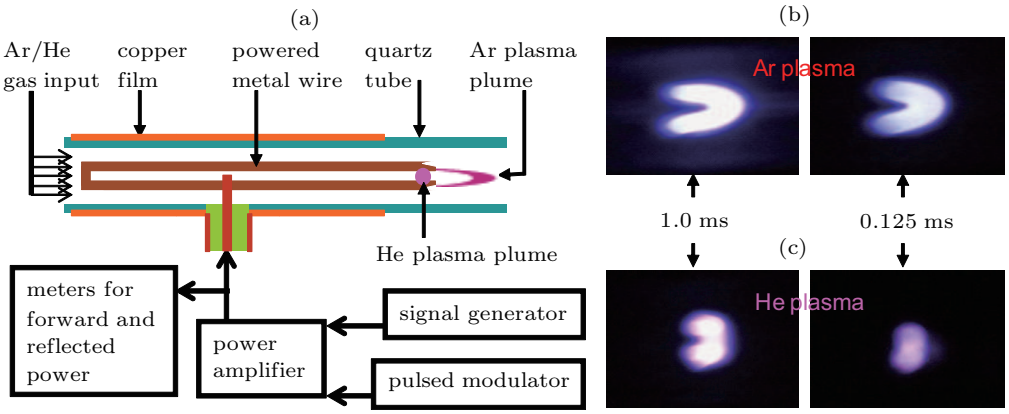


Fig. 1. (color online) (a) Schematic of the experimental system. Photo images of (b) Ar plasma and (c) He plasma are taken with maximum power of 5 W, pulsed frequency of 10 kHz, duty cycle of 0.2, and gas flow rate of 1.0 slm.

3. Results and discussion

3.1. Distinctive plasma plume morphologies

When Ar gas flow of 1.0 slm and microwave pulses are applied on the hairpin resonator, an arched plasma plume can be generated at the opened end of the hairpin resonator. Figure 2 shows a group of discharge images captured by the ICCD camera. The pulsed frequency of 10 kHz, duty ratio of 0.2, and pulsed power of 5 W are maintained. Hence each pulse has a time of 20 μs with microwave power and 80 μs without microwave power. As shown in Fig. 2, during the first 1 μs from 0 to 1 μs, the arched lightened pattern seems dim, suggesting that it is the afterglow of the previous discharge. In the time of 1–2 μs, a light point appears at the tip of the main electrode. At about the time of 3 μs, the ionization develops to the slave electrode and thereafter the more lightened arched pattern is formed. From 4 μs

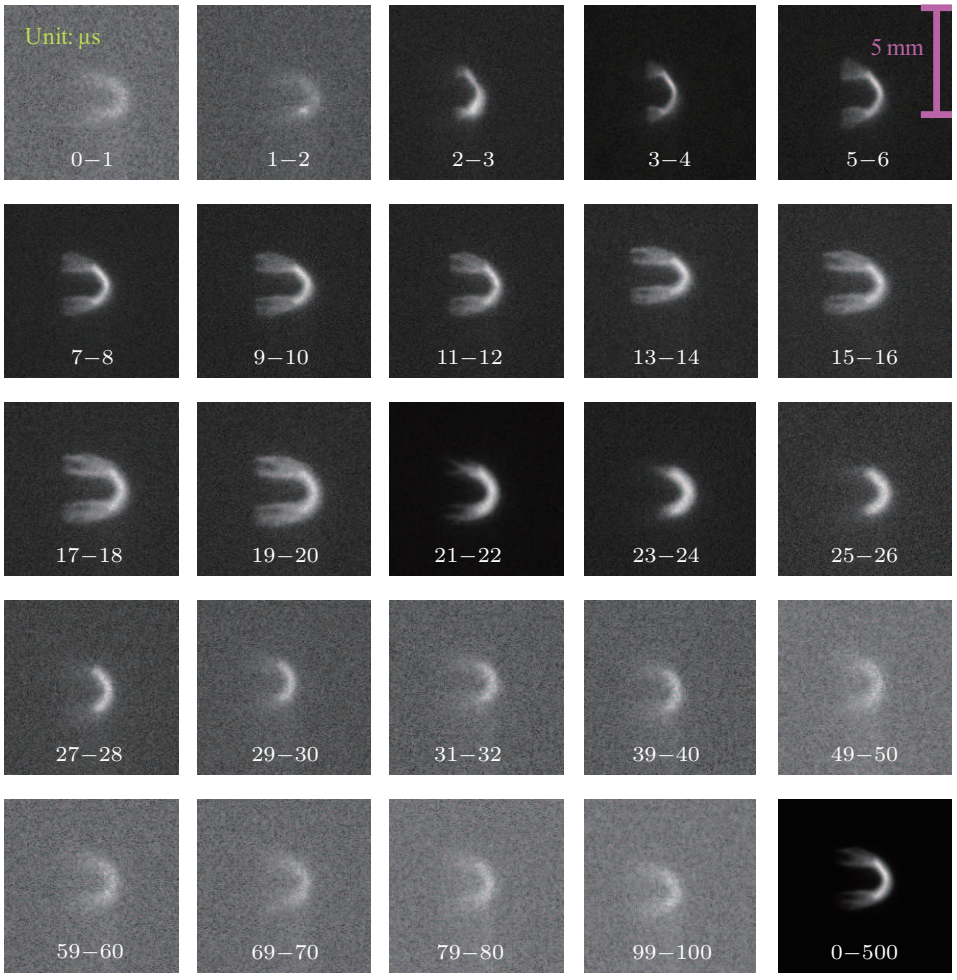


Fig. 2. (color online) Sequence of discharge images obtained using the ICCD camera with different exposure times. The time spans are indicated in each image. A pulse frequency of 10 kHz, duty cycle of 0.2, peak input power of 5 W, and an argon gas flow of 1.0 slm are used.

to 20 μs, the thickness of plasma plume grows and the discharge domain stretches backward to both powered electrodes. In the time of 21–24 μs, the discharge domains around the metal wires decay, but the forward arched plume becomes stronger in light intensity. After 25 μs till the next pulse, the discharge comes into the afterglow period and the light intensity damps more and more weakly. In order to check how long the afterglow of microwave Ar plasma could persist, we reset the pulsed frequency of 2 kHz, the duty ratio of 0.1, and the pulsed power of 8 W. Then for each pulse microwave power on time changes to 50 μs and microwave power off time reaches 450 μs. Figure 3 shows this group of discharge images. In comparison to Fig. 2, the discharge process and the distinctive formation are similar. It should be mentioned that the afterglow of microwave Ar plasma plume can persist longer than 450 μs, which is the longest time for the afterglow of Ar APPJ as far as we know.

Moreover, in combination with Figs. 2 and 3, the ionization process of pulsed microwave Ar APPJ could be divided into three develop phases, called reigniting, growing up, and finally shrinkage. At the reigniting phase, the microwave power rises higher than 2 W, then the electrons located at the tip of the powered electrode will be accelerated by the local enhanced electric field, and hot electrons collided frequently with Ar atoms will induce discharge. Due to the main electrode having stronger voltage, the ionization occurs at its tip firstly. Then the ionization process enters into the second phase of growing up. The ionization front develops along the previous discharge channel because there is an amount of Ar excitation state atoms and lower plasma density left in the afterglow. Once the arched discharge channel reignites in whole, the ionization domain will further occupy around the powered electrode tips, and meanwhile the forward arched plume grows thicker. In the final phase of shrinkage, the pump power disappears, and the electrons around the metal wire will be cold and be absorbed by electrodes quickly. The forward arched plume continues to be overdense about 5 μs because it has been heated too long and is with higher energy. In 5 μs after the microwave power is off, the forward arched Ar APPJ plume damps to very a weak state and waits for the next microwave pulse.

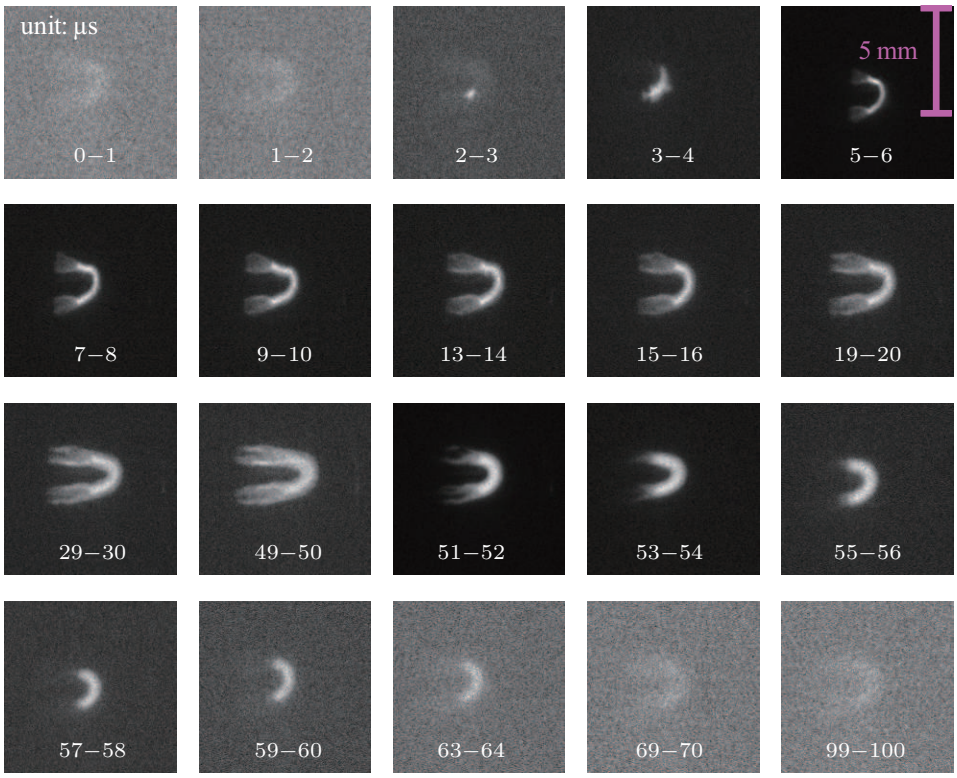


Fig. 3. (color online) A group of discharge images obtained by ICCD camera with exposure times of 1 μs. A pulse frequency of 2 kHz, duty cycle of 0.1, peak input power of 8 W, and an argon gas flow of 1.0 slm are used.

Next, we will continue to experiment on He discharge. Besides using He gas instead of Ar gas, the input parameters (pulsed frequency, duty ratio, microwave power, and gas flow) are set to the same as Ar discharges in order to compare each other. Figures 4 and 5 show the He discharge images, in which their input parameters are the same as those in Figs. 2 and 3, respectively. As shown in Fig. 4, the ionization starts at the inner side between both electrodes but near the main electrode at about 2 μs. After that time, the ionization front develops to the slave electrode and the discharge channel forms in be-

tween both electrodes. From 3 μs to 20 μs, the discharge channel becomes thicker. When the microwave pulse passes away, the He lightened discharge channel damps more quickly than Ar discharges besides that its middle domain of the discharge channel disappears at last. As for Fig. 5, the total situation is similar to Fig. 4 except that the reigniting stage is started somewhat slowly because there are little He atoms in the excitation state and lower electron density (shrinking too long).

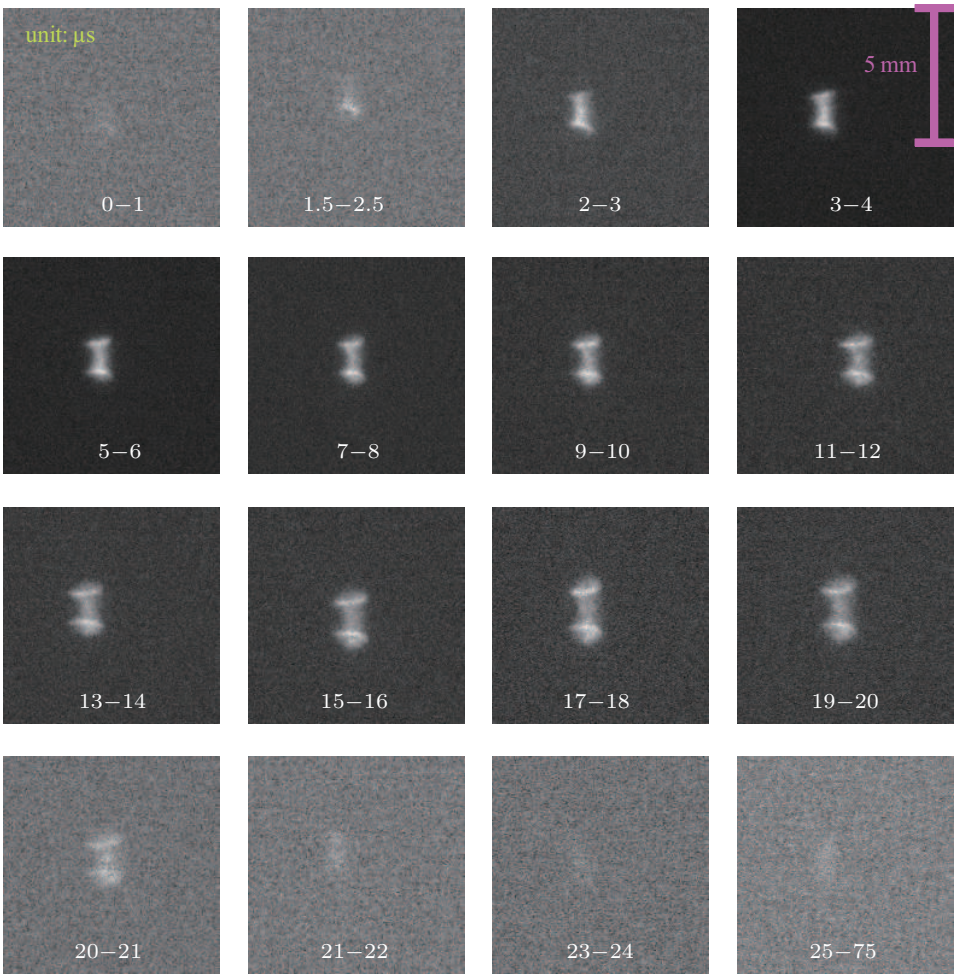


Fig. 4. (color online) A group of discharge images obtained by ICCD camera with the different exposure times. The discharge conditions are the same as those for Fig. 2 except using He gas instead of Ar gas.

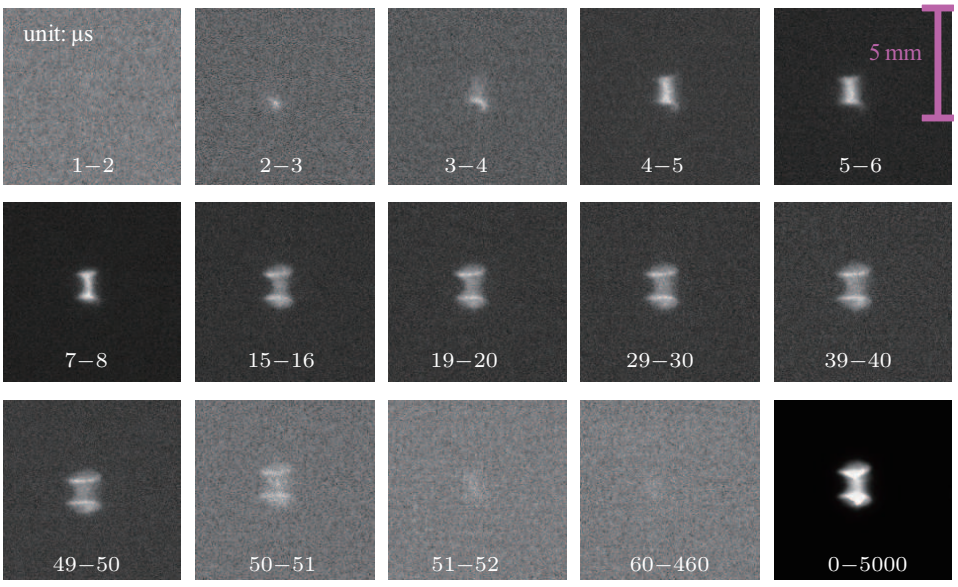


Fig. 5. (color online) Sequence of discharge images obtained by ICCD camera with the different exposure times. The discharge conditions are the same as those for Fig. 3 except using He gas instead of Ar gas.

In comparison with He discharge and Ar discharge, the main difference is that He plumes generate only a contracted plasmas in between both tips of the U-shaped powered electrode, whereas Ar plasmas form an arched plasma plume at the opened end of the hairpin resonator, as shown in Figs. 2–5. Despite this difference, their discharge processes have three similar characteristics: (i) the ionization occurs at the main electrode firstly and then develops to the slave electrode, (ii) during the shrinking stage the middle domains of the discharge channels disappear at last, and (iii) even at zero power input (in between pulses) a weak light region always exists at the discharge channels. The difference in discharge formation might be induced by the interaction between plasma plume and electric field or from the different ionization attributes of Ar/He gasous.[4,22,31]

3.2. Electromagnetic simulations

For an electromagnetic wave distributed in a transmission line, the input microwave power of 1 W will excite the maximum voltage amplitude of 10 V located at the opened end of the electrode. Without plasma load, the input voltage wave will be reflected from an opened end and should form a standing wave with a maximum voltage amplitude of 20 V.[22] The total length is three quarters of the wavelength and the discharge device resonates for the proposed hairpin resonator. The maximum voltage located at the opened end of the powered electrodes may get to 200 V.[27,28] The local enhanced electric field can easily ionize gas discharge. However, once the plasma load appears, the distribution of standing wave changes and the maximum voltage at the opened end loses probably. In order to study how the plasma load influences the distribution of standing wave, simple electromagnetic simulation models are developed by using a high-frequency structure simulator (HFSS, Ansoft). The detailed settings of our models can be referred in previous reports.[14,21,34,35]

Here, we will introduce the equivalent values of plasma parameters, which are input to the simulation model. In simulation, an equivalent dielectric is used to stand for plasma domain. HFSS simulator uses the electrical conductivity σ, relative permittivity $\varepsilon'_{\rm p}$, and dielectric loss tangent $\tan\delta$. Thence, we should deduce these three parameters from plasma parameters as[36–38]

$$\varepsilon_{\rm p} = \varepsilon'_{\rm p} + {\rm i}\varepsilon''_{\rm p} = 1 - \frac{\omega_{\rm p}^2}{\omega^2 + \nu_{\rm en}^2} + {\rm i}\frac{\omega_{\rm p}^2 \nu_{\rm en}}{\omega(\omega^2 + \nu_{\rm en}^2)}, \quad (1)$$

$$\sigma = {\rm i}\frac{n_{\rm e} e^2}{m_{\rm e}(\omega + {\rm i}\nu_{\rm en})}, \quad (2)$$

$$\tan\delta = \left|\varepsilon''_{\rm p}/\varepsilon'_{\rm p}\right|, \quad (3)$$

where ${\rm i} = \sqrt{-1}$ is the imaginary unit, $m_{\rm e}$ is the electron mass, e is the charge of an electron, ω is the angular frequency of microwave, $\nu_{\rm en} = 1.53 \times 10^{12}\sqrt{T_{\rm e}[{\rm eV}]}$ is the effective electron–neutral collision frequency, $T_{\rm e}[{\rm eV}]$ is the electron temperature in the unit of eV, $n_{\rm e}$ is the electron density, and $\omega_{\rm p} \approx 17.96\pi\sqrt{n_{\rm e}[{\rm m}^{-3}]}$ is the angular frequency of plasma electrostatic oscillation. So if we know the values of $T_{\rm e}[{\rm eV}]$ and $n_{\rm e}[{\rm m}^{-3}]$, by using Eqs. (1)–(3) $\varepsilon'_{\rm p}$, σ, and $\tan\delta$ can be counted, respectively. Our pervious simulation work had calculated step by step the distribution of $T_{\rm e}[{\rm eV}]$ and $n_{\rm e}[{\rm m}^{-3}]$ in the ionization process.[31] We select three typical data groups in terms of ($T_{\rm e}[{\rm eV}]$, $n_{\rm e}[{\rm m}^{-3}]$), like (0.05, 10^{17}), (0.1, 10^{21}), and (0.1, 10^{19}), representing the different discharge processes of 'pulse before', 'pulse on', and 'pulse after', respectively. Inputting them into Eqs. (1)–(3), another three digit groups in forms of ($\varepsilon'_{\rm p}$, σ, $\tan\delta$) can be approximated correspondingly as (1, 0.008, 0.064), (−13.6, 60, 34), and (0.85, 0.6, 5.4). For Ar plasma plume, an arched plasma domain with radius of 0.25 mm is set at the opened end of powered electrodes. As for He plasma, a cylindrical plasma domain with radius of 0.35 mm is arranged in between both electrode tips.

Figure 6 shows the simulated electric field distributions of Ar plasma model. Figure 6(a) gives the discharge process of 'pulse before' with the input power of 0.1 W and ($\varepsilon'_{\rm p}$, σ, $\tan\delta$) of (1, 0.008, 0.064). The standing wave is distributed along the powered electrodes and the electric fields are enhanced at the metal tips of both electrodes. The electric field located at the main electrode is stronger than that of the slave electrode. Figures 6(b) and 6(c) present the discharge processes of 'pulse on', where ($\varepsilon'_{\rm p}$, σ, $\tan\delta$) is selected as (−13.6, 60, 34) but the input powers are applied in 3 W and 5 W, respectively. At the pulse rise time about 3 μs (corresponding to 3 W), the discharge process is in the phase of reigniting, and thence a half of the arched plasma domain is set at the tip of the main electrode. Comparing Fig. 6(b) with Fig. 6(c), the strongest electric field is placed at the up end of the half arched plasma domain as shown in Fig. 6(b), while the end of the main electrode again obtains the maximum value of electric field as shown in Fig. 6(c). Figure 6(d) displays the discharge process of 'pulse after' with the input power of 0.5 W and only a forward arched plasma domain with parameter ($\varepsilon'_{\rm p}$, σ, $\tan\delta$) of (0.85, 0.6, 5.4). As shown in Fig. 6(d), the standing wave pattern forms due to the plasma density being too weak.

As for an electromagnetic simulation of the He gas discharge process, we change the location of the plasma domain. Figure 7 shows four kinds of simulated electric field distributions corresponding to the different discharge processes of 'pulse before', 'pulse on', and 'pulse after', respectively. Also the parameters used in Fig. 7 correspond to those used in Fig. 6. Despite their differences in the details, the standing waves distribute along the electrode and the strongest electric fields take place at the opened end of the hairpin resonator.

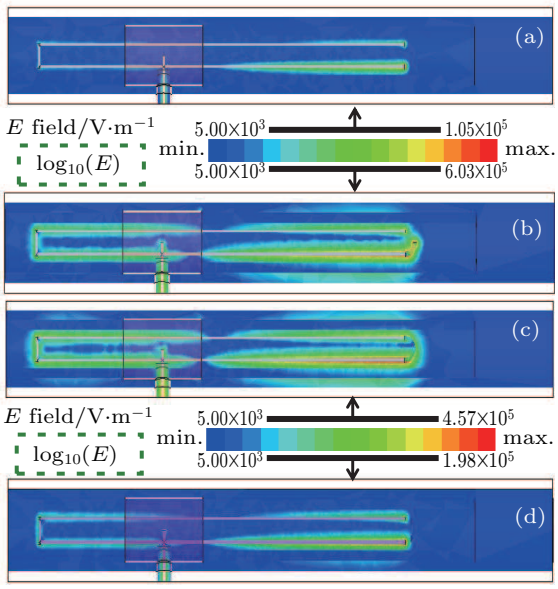


Fig. 6. (color online) Simulated electric field distributions for Ar plasmas with different plasma domains or different plasma parameters.

We also sample the simulated electric field distributions in one microwave period. Figure 8 shows the simulated results varied along with the different microwave phases. The plasma parameters used in Fig. 8(a) and Fig. 8(b) are the same as those in Fig. 6(c) and Fig. 7(c) representing Ar discharge and He discharge, respectively. It is interesting to note that a hollow shape of the electric field distributed in the plasma domains is always exhibited in disregard of the microwave phases and gas discharges, as shown in Fig. 8. This character suggests that conduction within the discharge channel is sufficiently strong that the microwave energy can be able to conduct through the plasma jet plume between the powered electrodes. As shown in Fig. 8, another interesting point is at phase 0.25π the enhanced electric field emerging around the plasma domain, which indicates that the standing wave mode located at the plasma domain is the SPPs.[38] At the transient state of phase 0.25π, the standing wave mode is pure SPPs. We can conceive that at other phase states the standing wave mode would be the hybrid wave of an electromagnetic wave plus the SPPs. The electromagnetic standing wave is driven by the input microwave and locates along the metal electrode of the hairpin resonator, while the standing wave of SPPs merely takes place at the dielectric with negative refractive index like plasma domain as the frequency of plasma electrostatic oscillation is larger than the frequency of pumping wave. Although both waves are with the different attributes, their wave modes belong to transverse magnetic (TM) modes and they can be transformed to each other by wave mode transforming.[37,38]

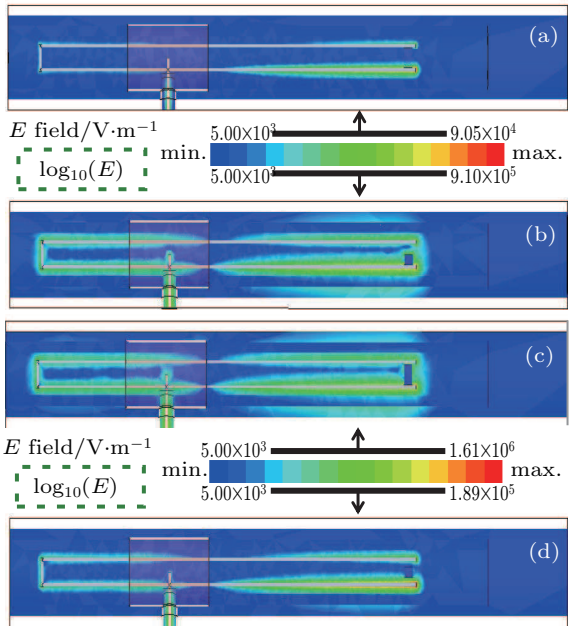


Fig. 7. (color online) Simulated electric field distributions for He plasmas with different plasma domains or different plasma parameters.

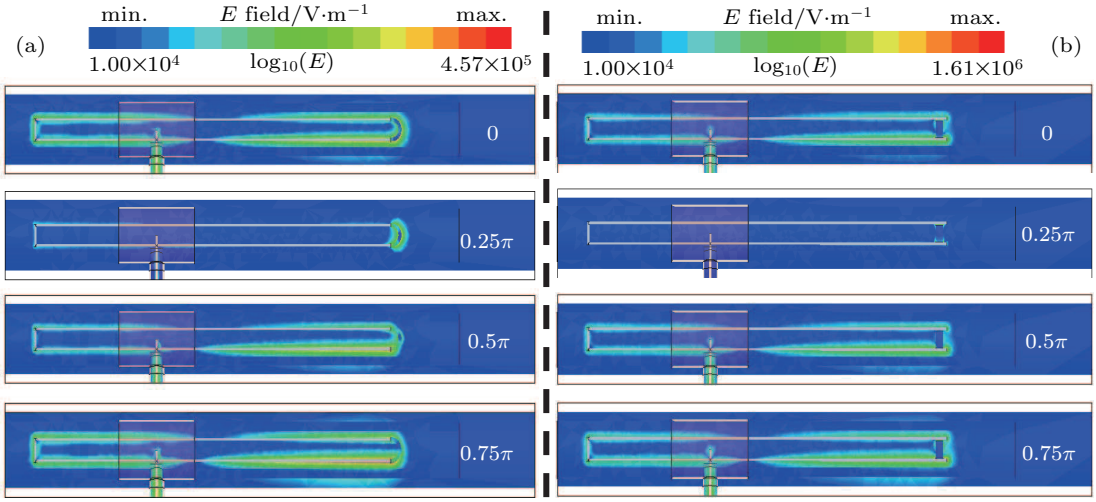


Fig. 8. (color online) Simulated electric field distributions with the different microwave phases for (a) Ar plasmas and (b) He plasmas, respectively.

3.3. Discussion on the discharge process

Combining the discharge images with the electromagnetic simulations, the ionization process and the characteristic morphologies of atmospheric Ar and He plasmas should be analyzed. Before discharge, once the input microwave is applied on the hairpin resonator, the standing electromagnetic wave would be formed and the maximum electric field should be located at the opened end of electrodes. Due to the larger gap of 2 mm, in experiment we often need to apply a microwave power higher than 6 W to ignite the discharge. After the igniting started, the applied microwave power could be decreased to a lower value but higher than 2 W, which suggests that the previous discharge can active the latter ionization process. We assume that the influence factor is the afterglow effect. Because of the main electrode with much stronger electric field, the reigniting would easily happen there, which has been verified by experiment as shown in Figs. 2–5 (at about 3 μs) and by simulations as indicated in Figs. 6(a) and 7(a). At atmospheric gas pressure, the ionization is governed by streamer theory and the developed electron avalanche performs as an ionization wave (plasma bullet), which has an enhanced static electric field at its head part, called the ionization front.[1–3] In addition, the proposed hairpin resonator is with three quarters wavelength and both tips of electrodes have maximum voltages with opposite polarities. Thence, the inner domain between both electrodes has much stronger electrodes, which would favor the ionization direction developing from the main electrode to the slave electrode. At about 4 μs, the discharge channel forms at the opened ends of both electrodes. After that stage, on the one hand the discharge channel becomes thicker; on the other hand the discharge develops backwards to electrodes till to the microwave pulse damping. The discharge development is still induced by the changeable stronger electric field distributions as shown in Figs. 6(c) and 7(c). Once the pumping microwave pulse disappears, the discharge domain around the metal electrodes will decrease quickly because of the thinner sheath region at atmospheric discharges and sheath region damping quickly. The middle domain of the discharge channel shrinks at last also due to this effect in part, and another reason might be the plasma maintained by SPPs for a longer time. There exists wave mode coupling among standing electromagnetic wave, SPPs, and static plasma electron wave.[37,38] When the input microwave pulse is applied, the order of wave mode transform is from the standing electromagnetic wave to SPPs and thereafter from SPPs to the static plasma electron wave. The electrons accelerated by the electric field of the static plasma electron wave become hot and thereby advance the ionization development. When the input microwave pulse is passed, the transform order might be from the static plasma electron wave to SPPs, then from SPPs to the standing electromagnetic wave and finally wave modes transformation conversely. From the view of energy conservation, the microwave power is mainly consumed by the plasma plume. That is to say, the wave mode coupling can delay the ionization development. This effect can be used to interpret the middle domain of the discharge channels disappearing at last, as shown in Figs. 2–6.

The above discharge processes are the common characteristics of the hairpin resonator despite Ar discharge or He discharge. But as for why they perform different plasma plume patterns, the different ionization and excitation energies and the gas flow effects for Ar and He atoms might be two main affected factors.[39–41] As is well known, the molecular weight of Ar atom is far more than that of He atom and the effect of Ar gas flow is far greater than that of He gas. In our previous experiment, we have observed that the radian of the arched Ar plasma plume is mainly affected by the gas flow rate.[31] The develop direction of the ionization front is from the main electrode to the slave electrode, while the gas flow direction is along the axis of the quartz tube. So the arched Ar plasma plume pattern forms. For He plasma, however, it is mainly affected by the direction of strong electric field and the He discharge channel is merely in existence between the inner part of both electrodes. Moreover, the different ionization and excitation energies for Ar and He atoms also affect the formation of discharge morphologies. Actually, the electron density of the hairpin resonator is in the amplitude of 10^{21} m^{-3}. Even at its shrinking stage, the electron density is still approximated in the order of 10^{19} m^{-3}.[22,31] Under these intense conditions for atmospheric Ar plasma, the Ar^* (argon metastable) population would be strongly depleted from the center of the discharge channel due to two-step ionization.[27] The depletion of Ar^* from the center of the discharge channel would induce the reducing of visible emission.[4,28] In other words, the energy damping used for light emission would be reduced and the lightened arched domain could exist with the weak light region in the discharge channel even at zero power input (in between pulses). For Ar microwave APPJ, Ar^* populations located around the discharge channel are more intense,[40] the Ar^* lifetime is longer than 400 μs, and its afterglow is too intense to shrink immediately in view of space and time, which in all induce the formation of the arched plasma plume morphology. As for He microwave discharge, on the one hand, the plasma shrinking quicker than Ar plasma is due to its ionization energy being much higher than that of Ar atom.[41] At the shrinking stage, the local enhanced electric field weakens much more quickly to lower than the threshed value that could ionize the He atoms. On the other hand, the He APPJ might

not suffer from metastable depletion and the energy damping used for light emission would be more quickly.[27,42,43] The energetic electrons that can ionize He atoms are only generated in between both tips of the metal electrodes, and thence only a contracted discharge occurs, as shown in Figs. 4–5.

4. Conclusion

The ionization process and the characteristic morphologies of atmospheric Ar and He plasmas excited by a pulsed microwave hairpin resonator have been studied. In discharge experiments, the discharge images show that Ar plasmas form an arched plasma plume at the opened end of the hairpin, whereas He plumes generate only contracted plasmas in between both tips of metal electrodes. As shown in discharge images captured by the ICCD camera, the discharge processes have three similar characteristics in spite of whether Ar or He discharges are used: (i) the ionization occurs at the main electrode firstly and then develops to the slave electrode, (ii) during the shrinking stage the middle domain of the discharge channels disappear at last, and (iii) even at zero power input (in between pulses) a weak light region always exists in the discharge channels. Combining the experimental results and the electromagnetic simulations, we conclude that the discharge is resonantly excited by the local enhanced electric fields distributed in a hairpin resonator. In addition, because Ar ionization and excitation energies are lower than those of He, the effect of Ar gas flow is far greater than that of He gas, the contribution of accelerated electrons only locates at the place with the strongest electric fields, the wave mode coupling could maintain the ionization development for a longer time, and the Ar^* population would be strongly depleted from the center of the discharge channel but not for He discharges. These effects together could generate the different characteristic plume morphologies of the proposed atmospheric Ar and He plasmas.

To focus more attention on the present interesting study, there still exist several opening questions that are valuable for future investigations. For example, in experiment we have done the microwave discharge with two electrodes in a free-space gap of 2 mm. Whether there has a larger gap in free space that could be constructed for microwave discharge is a more interesting study point due to the much longer discharge channel being capable of indicating the ionization process clearly in space. In simulation, the present electromagnetic model is somewhat too simple. Although we have taken the plasma parameters varied with the ionization development into account, the self-interaction between the development of plasma plume and the input microwave power is much more complicated. A more sophisticated simulation model is still in training and reorganizing from our previous models. Maybe a self-consistent fluid model [31,32,44–49] or a particle-in-cell model plus Monte Carlo calculator (PIC/MCC) [22,50–56] could indicate much more physical information for hairpin resonators.

References

[1] Lu X, Naidis G V, Laroussi M and Ostrikov K 2014 *Phys. Rep.* **540** 123
[2] Lu X, Naidis G V, Laroussi M, Reuter S, Graves D B and Ostrikov K 2016 *Phys. Rep.* **630** 1
[3] Lu X, Laroussi M and Puech V 2012 *Plasma Sources Sci. T.* **21** 034005
[4] Lee H W, Kang S K, Won I H, Kim H Y, Kwon H C, Sim J Y and Lee J K 2013 *Phys. Plasmas* **20** 123506
[5] Urabe K, Morita T, Tachibana K and Ganguly B 2010 *J. Phys. D-Appl. Phys.* **43** 095201
[6] Yue Y, Wu F, Cheng H, Xian Y, Liu D, Lu X and Pei X 2017 *J. Appl. Phys.* **121** 033302
[7] Wu S, Huang Q, Wang Z and Lu X 2011 *IEEE T. Plasma Sci.* **39** 2286
[8] Sakiyama Y, Graves D, Jarrige J and Laroussi M 2010 *Appl. Phys. Lett.* **96** 041501
[9] Naidis G V 2011 *J. Phys. D-Appl. Phys.* **44** 215203
[10] Boeuf J, Yang L and Pitchford L 2013 *J. Phys. D-Appl. Phys.* **46** 015201
[11] Breden D, Miki K and Raja L 2012 *Plasma Sources Sci. T.* **21** 034011
[12] Munoz J and Calzada M D 2008 *J. Phys. D-Appl. Phys.* **41** 135203
[13] Takamura S, Amano S, Kurata T, Kasada H, Yamamoto J, Razzak M A, Kushida G, Ohno N and Kando M 2011 *J. Appl. Phys.* **110** 043301
[14] Chen Z, Xia G, Zhou Q, Hu Y, Zheng X, Zheng Z, Hong L, Li P, Huang Y and Liu M 2012 *Rev. Sci. Instrum.* **83** 084701
[15] Chen Z, Liu M, Xia G and Huang Y 2012 *IEEE T. Plasma Sci.* **40** 2861
[16] Hnilica J, Kudrle V, Vasina P, Schafer J and Aubrecht V 2012 *J. Phys. D-Appl. Phys.* **45** 055201
[17] Chen C, Li S, Wu Y, Li Z, Zhang J and Wang Y 2016 *Phys. Plasmas* **23** 123501
[18] Kang S K, Kim H Y, Yun G S and Lee J K 2015 *Plasma Sources Sci. T.* **24** 035020
[19] Choi J, Iza F, Do H J, Lee J K and Cho M H 2009 *Plasma Sources Sci. T.* **18** 025029
[20] Chen Z, Liu X, Zou C, Song X, Li P, Hu Y, Qiu H, Kudryavtsev A A and Zhu M 2017 *J. Appl. Phys.* **121** 023302
[21] Chen Z, Xia G, Zou C, Liu X, Feng D, Li P, Hu Y, Stepanova O and Kudryavtsev A A 2017 *J. Appl. Phys.* **122** 093301
[22] Hopwood J, Hoskinson A R and Gregório J 2014 *Plasma Sources Sci. T.* **23** 064002
[23] Wu C, Hoskinson A R and Hopwood J 2011 *Plasma Sources Sci. T.* **20** 045022
[24] Hoskinson A R and Hopwood J 2012 *Plasma Sources Sci. T.* **21** 052002
[25] Zhang Z and Hopwood J 2009 *Appl. Phys. Lett.* **95** 161502
[26] Gregório J, Hoskinson A R and Hopwood J 2015 *J. Appl. Phys.* **118** 083305
[27] Monfared S K, Hoskinson A R and Hopwood J 2013 *J. Phys. D-Appl. Phys.* **46** 425201
[28] Miura N and Hopwood J 2011 *J. Appl. Phys.* **109** 113303
[29] Hoskinson A R, Gregório J, Hopwood J, Galbally-Kinney K L, Davis S J and Rawlins W T 2017 *J. Appl. Phys.* **121** 153302
[30] Kang S K, Seo Y S, Lee H W, Aman-ur-Rehman, Kim G C and Lee J K 2011 *J. Phys. D-Appl. Phys.* **44** 435201
[31] Chen Z, Xia G, Zou C, Li P, Hu Y, Ye Q, Eliseev S, Stepanova O, Saifutdinov A I, Kudryavtsev A A and Liu M 2015 *J. Appl. Phys.* **118** 023307
[32] Chen Z, Yin Z, Chen M, Hong L, Xia G, Hu Y, Huang Y, Liu M and Kudryavtsev A A 2014 *J. Appl. Phys.* **116** 153303
[33] Chen Z, Yin Z, Xia G, Hong L, Hu Y, Liu M, Hu X and Kudryavtsev A A 2015 *Chin. Phys. B* **24** 025203
[34] Chen Z, Yin Z, Huang Y, Stepanova O, Gutsev S and Kudryavtsev A A 2015 *IEEE T. Plasma Sci.* **43** 906
[35] Chen Z, Hu D, Liu M, Xia G, Zheng X, Hu Y, Ye Q, Chen M, Zhu L and Hu X 2014 *Chin. Phys. B* **23** 035202
[36] Raizer Y P 1991 *Gas Discharge Physics* (Berlin: Springer)
[37] Raether H 1988 *Surface Plasmons* (New York: Springer)

[38] Kalluri D K 2011 *Electromagnetic Waves, Materials, and Computation with MATLAB* (Taylor & Francis Group)

[39] Carbone E, Hubner S, Palomares J M and Mullen M van der J A 2012 *J. Phys. D-Appl. Phys.* **45** 345203

[40] Carbone E and Nijdam S 2014 *Plasma Sources Sci. T.* **23** 012001

[41] Carbone E, Sadeghi N, Vos E, Hubner S, Veldhuizen van E, Dijkvan J, Nijdam S and Kroesen G 2015 *Plasma Sources Sci. T.* **24** 015015

[42] Liu X, Pei X, Lu X and Liu D 2014 *Plasma Sources Sci. T.* **23** 035007

[43] Yue Y, Xian Y, Pei X and Lu X 2016 *Phys. Plasmas* **23** 123503

[44] Hoskinson A R, Gregório J, Parsons S and Hopwood J 2015 *J. Appl. Phys.* **117** 163301

[45] Kourtzanidis K, Boeuf J P and Rogier F 2014 *Phys. Plasmas* **21** 123513

[46] Gregório J, Parsons S and Hopwood J 2016 *Plasma Sources Sci. T.* **25** 035018

[47] Zhao G L, Hua W, Guo S Y and Liu Z L 2016 *Phys. Plasmas* **23** 073503

[48] Zhang D, Zhou R, Yang X Q and Wu S Y 2016 *Phys. Plasmas* **23** 073504

[49] Chu H, Ren F, Feng Y, Gu M and Zheng S 2017 *Appl. Therm. Eng.* **124** 362

[50] Levko D and Raja L L 2016 *J. Appl. Phys.* **119** 163303

[51] Levko D and Raja L L 2015 *J. Appl. Phys.* **118** 043303

[52] Chen Z, Ye Q, Xia G, Hong L, Hu Y, Zheng X, Li P, Zhou Q, Hu X and Liu M 2013 *Phys. Plasmas* **20** 033502

[53] Chen Z, Yin Z, Chen M, Liu M, Xu G, Hu Y, Xia G, Song X, Jia X and Hu X 2014 *Acta Phys. Sin.* **63** 095205 (in Chinese)

[54] Kwon H C, Jung S Y, Kim H Y, Won I H and Lee J K 2014 *Phys. Plasmas* **21** 033511

[55] Chen Z, Xia G, Liu M, Zheng X, Hu Y, Li P, Xu G, Hong L, Shen H and Hu X 2013 *Acta Phys. Sin.* **62** 195204 (in Chinese)

[56] Zhu L, Chen Z, Yin Z, Wang G, Xia G, Hu Y, Zheng X, Zhou M, Chen M and Liu M 2014 *Chin. Phys. Lett.* **31** 035203